Rugae-like Ni$_2$P-CoP nanoarrays as a bi-functional catalyst for hydrogen generation: NaBH$_4$ hydrolysis and water reduction

Jingya Guo[a,1], Benzhi Wang[a,1], Dandan Yang[a], Zixia Wan[a], Puxuan Yan[a], Jianniao Tian[a], Tayirjan Taylor Isimjan[b,*], Xiulin Yang[a,*]

[a] Guangxi Key Laboratory of Low Carbon Energy Materials, School of Chemistry and Pharmaceutical Sciences, Guangxi Normal University, Guilin, 541004, People's Republic of China
[b] Saudi Arabia Basic Industries on (SABIC) at King Abdullah University of Science and Technology (KAUST) Saudi Arabia

ARTICLE INFO

ABSTRACT

Designing a bifunctional catalyst that performs hydrolysis of metal hydrides and water reduction spontaneously is an essential step towards developing an integrated H$_2$ storage system. Herein, a series of rugae-like CoP-Ni$_2$P arrays decorated Ni foam (Ni-Co$_x$-P@NF) are fabricated by two-step electrodeposition followed by phosphating treatment. The optimized Ni-Co$_{20}$-P@NF catalyst shows a superior catalytic H$_2$ generation by NaBH$_4$ hydrolysis, giving a specific H$_2$ generation rate of 4323.0 mL min^{-1} g^{-1} catalyst and good reusability, far better than most previously reported catalysts. Besides, the catalyst also exhibits an excellent electrocatalytic hydrogen evolution reaction with a low overpotential of 67.0 mV to reach -10 mA cm^{-2}, small Tafel slope and long-term stability in 1.0 M KOH. The outstanding catalytic H$_2$ generation capacity is attributed to the synergistically catalytic effect between the Ni$_2$P and CoP species, as well as the unique composite structure with the benefit of solute transport and gas emission.

1. Introduction

Hydrogen (H$_2$) is clean energy sources that regarded as a future replacement of fossil fuel due to the highest energy per mass 142 MJ kg^{-1} [1]. As an alternative of methane reforming, the electrochemical water splitting attracts a lot of attention due to the zero carbon emission and high purity H$_2$. Most importantly, H$_2$ can be generated using renewable energy such as solar and wind. However, the electrochemical water splitting requires a much higher voltage (1.8 ~ 2.0 V) than the theoretical limit of 1.23 V owing to the strong uphill reaction that requires high overpotentials [2]. As a result, it is critical to developing the efficient electrocatalysts that improve the sluggish kinetics thereof decrease the overpotential. The state-of-the-art hydrogen evaluation reaction (HER) catalysts are based on the expensive noble metal Pt [3,4]. Hence, extensive efforts have been devoted to developing robust and cheap noble-metal-free transition metal catalyst including sulfides, selenides, phosphides, carbides, and nitrides, *etc.* [5]. Among them, the increasing attention has been paid to metal phosphides (Ni$_2$P, CoP, MoP, and FeP) as HER catalyst because of the thermostability, high conductivity, and low cost [6]. Besides, the metal phosphides show bulk activity as compare to the metal sulfides of which the electrocatalytic

activity is limited to the edges [7]. Thus the metal phosphides often show better HER performance compare to those of others. Therefore, self-supported metal phosphide nanostructures *in situ* grown on 3D substrates have been widely exploited because the self-supported HER catalyst has several advantages as compared to a powder-based catalyst such as no binder, more active sites, better charge transfer and easy to be prepared [8–10]. However, the long term stability of the metal phosphides based HER catalyst is the primary concern.

Apart from the H$_2$ production, the H$_2$ storage is also a critical process for a sustainable "hydrogen economy". H$_2$ storage is particularly challenging because of its low volumetric energy density. In general, there are two categories for storage H$_2$ including physical and chemical methods [11]. The physical storage based on forming either the high pressure (350 ~ 700 bar) compressed gas or low-temperature liquid. The hydrogen can also be stored on the surface of porous scaffolds through physical absorption, for example, organic frameworks and polymers with intrinsic porosity [12,13]. On the other hand, the chemical storage is realized by a reversible chemical bonding between hydrogen and absorbents including liquid organic (HCOOH) [14–16], interstitial metal hydride (LaNiH$_6$) [17], complex hydride (NaAlH$_4$) [18–20], and chemical hydride (NaBH$_4$) [21,22].

However, developing high-density hydrogen storage for stationary and portable applications remains a significant challenge. Among all the chemical storage materials, chemical hydrides ($NaBH_4$, NH_3BH_3, and $LiBH_4$) are the best candidate in this regard because of the high hydrogen gravimetric storage capacity, stable chemical properties, and non-toxicity [23–25]. Nevertheless, boron hydride hydrolysis generally suffers from sluggish reaction kinetics. At present, platinum-based materials are the best performing catalysts for hydrolysis of sodium borohydride [26,27] and a lot of efforts have been made to develop the earth's abundant non-noble metal catalysts to replace the expensive platinum-based catalysts [28,29]. Among them, transition metal phosphides such as CoP/C nanoboxes [30], CoP_2 nanowire [31], $Ni_2P@Ni$-$FeAlO_x$ [32], Ni − Cu − P nanotube [33], CoP/NiCoP [34], etc. become the hotspot. Wang et al. [35] and Zhang et al. [36] found that the bimetallic phosphides can significantly improve the catalytic performance as compared to single metal phosphides due to the synergistic effect. The maximum solubility of $NaBH_4$ in water is around 25 % therefore only a quarter of the $NaBH_4$ solution is consumed after $NaBH_4$ hydrolysis which means 75 % of the water is wasted.

Herein, we proposed a bifunctional Ni_2P-CoP catalyst that can be used spontaneously for $NaBH_4$ hydrolysis and HER catalyst (cathode) for water splitting. In another word, we can design a system that couples $NaBH_4$ hydrolysis with water splitting to maximize the H_2 extraction from both $NaBH_4$ and alkaline water solution. In this goal, we fabricated the rugae-like Ni_2P-CoP arrays decorated Ni foam catalyst by the integrating two-step electrodeposition followed by a vapor phase phosphatization. The optimized Ni-Co_{20}-P@NF exhibits an outstanding catalytic performances towards $NaBH_4$ hydrolysis and HER in two separate system. Moreover, it also shows excellent reusability and long-term stability. The superior H_2 production capacity can be explained by the following two aspects including the hierarchical porous structures resulted in abounded active sites and better mass transfer [37] as well as the synergetic effect between Ni_2P and CoP species [38].

2. Experimental section

2.1. Synthesis of Ni-Co$_x$-species@NF

All chemicals are analytical grade and do not require further purification in experiments. Firstly, pretreatment of the nickel foam (1 cm × 1 cm × 1.6 mm) with 1.0 M HCl, deionized water and ethanol for 5 min respectively, and then repeated 3 times to make sure the surface of the NF was well cleaned. To prepare the Ni-Co-species@NF, 1.0 mmol of $Co(NO_3)_2·6H_2O$ and 1.0 mmol of $Ni(NO_3)_2·6H_2O$ was ultrasonically dissolved into 40 mL deionized water to form uniform solutions, respectively. The electrodeposition experiments were carried out at room temperature in a standard three-electrode system to electrodeposit Co-species and Ni-species in sequence. The NF skeleton was used as the working electrode, a Pt sheet and a saturated calomel electrode SCE electrode used as the counter electrode and the reference electrode respectively. A series of composites with different Co/Ni molar ratios were synthesized by changing the deposition times at a constant current density of -10 mA cm^{-2}, in which the total electrodeposition time is kept at 1.0 h. After being thoroughly washed and dried at room temperature, the resulted products were labeled as Ni-Co$_x$@NF (x = 5, 10, 15, 20 and 25).

We prepared a series of control materials by changing one parameter at a time. First, the order of electrodeposition of Co/Ni was reversed, while the ratio of Ni/Co was kept at 1/20 (Co$_{20}$-Ni@NF). Second, a mixture of Ni-Co solution was prepared with the molar ratio of Ni/Co for 1/20 [(Co$_{20}$Ni)@NF]. Third, only Co or Ni species was electrodeposited on the surface of NF (Co@NF and Ni@NF). All of the above experiments were performed at -10 mA cm^{-2} for a total deposition time of 1.0 h.

2.2. Synthesis of Ni-Co$_x$-P@NF by vapor phase phosphidation

The phosphidation process was performed in a tube furnace, where a porcelain boat containing NaH_2PO_2 as a phosphorus source was placed upstream, and all electrodeposited products were placed in another porcelain boat placed downstream. The furnace was heated to 350 °C with 2 °C min^{-1} in Ar atmosphere (20 sccm), and kept at 350 °C for 2 h. After the phosphidation, the samples were cooled down to ambient temperature in flowing Ar gas. Thereafter, a series of samples were prepared and named as Ni-Co$_x$-P@NF (x = 5, 10, 15, 20 and 20), Co$_{20}$-Ni-P@NF, (Co$_{20}$Ni)P@NF, CoP@NF and Ni$_2$P@NF, etc., as the following studies.

As a control, commercial Pt/C modified NF was also prepared, where 10.0 mg of commercial 20 wt% Pt/C powder was ultrasonically dispersed in 0.5 ml of 0.2 wt% Nafion solution. After 30 min, the resulted mixture was pipetted onto the surface of NF (1 cm × 1 cm) and dried naturally in air.

2.3. Characterizations

The crystal structures of catalysts were analyzed by X-ray powder diffraction (XRD, Rigaku D/Max 2500 V/PC) with a sweep speed for 2.0 ° min^{-1}. The morphologies and microstructures of the catalysts were characterized by scanning electron microscope (SEM, FEI Quanta 200 FEG) and transmission electron microscope (TEM, JEM-2100 F). The X-ray photoelectron spectrometer (XPS, JPS-9010 Mg Kα) was used to analyze the chemical states of different elements. The actual loadings of different metals in the catalyst were checked by inductive coupled plasma atomic emission spectroscopy (ICP-AES, IRIS Intrepid II XSP). The specific BET surface area of the as-prepared materials were measured on Quantachrome instrument. The conductivity of various materials were tested by four-point probe meter (RTS-9).

2.4. Catalytic hydrolysis of sodium borohydride studies

The catalytic activity, cycle stability and activation energy of the catalytic material were obtained by the following methods. Typically, 50 mL mixture solution (contained 150 mM $NaBH_4$ + 0.4 wt% NaOH) was kept in a three-necked round-bottom flask (100 mL), which was placed in a water bath at 25 °C. The volume of H_2 was monitored by a drainage which was connected to a computer to record the instantly changed water quantity. The catalytic reaction was started when the catalyst was added into the flask under constant magnetic stirring conditions. In order to test the recyclability of the catalyst, we continued to use the fresh $NaBH_4$ solution instead of the fully decomposed $NaBH_4$ solution for five consecutive cycles at 25 °C. After each stability test, we centrifuged the catalytic material, dried it under vacuum condition at room temperature, and weighed the catalytic material. All experiments were repeated three times to ensure the reliable results. The activation energy of the designed catalyst was evaluated in the same device in the temperature range of 25–45 °C.

2.5. Electrochemical hydrogen evolution studies

The electrocatalytic performance of different catalysts were performed in a standard three-electrode system with a Multi-channel electrochemical workstation (Bio-logic VMP3, France) at room temperature. The graphite plate and a saturated calomel electrode (SCE) were used as counter and reference electrodes, respectively. Cyclic voltammetry (CV) tests were firstly carried out for about 3～5 cycles to stabilize the electrocatalytic performance of the catalyst at a scan rate of 20 mV s^{-1}. Then, liner sweep voltammetry (LSV) curves were performed at a scan rate of 5 mV s^{-1}, and electrochemical impedance spectroscopy (EIS) was evaluated near the onset potential in the frequency range from 200 kHz to 10 mHz. Cyclic voltammetry (CV) method was used to derive the electrochemical double-layer

capacitance (C_{dl}) in a non-Faradaic potential window. The electrochemical double-layer is similar to the regular capacitors where the energy stored in the C_{dl} by simply charge separation. Therefore, the
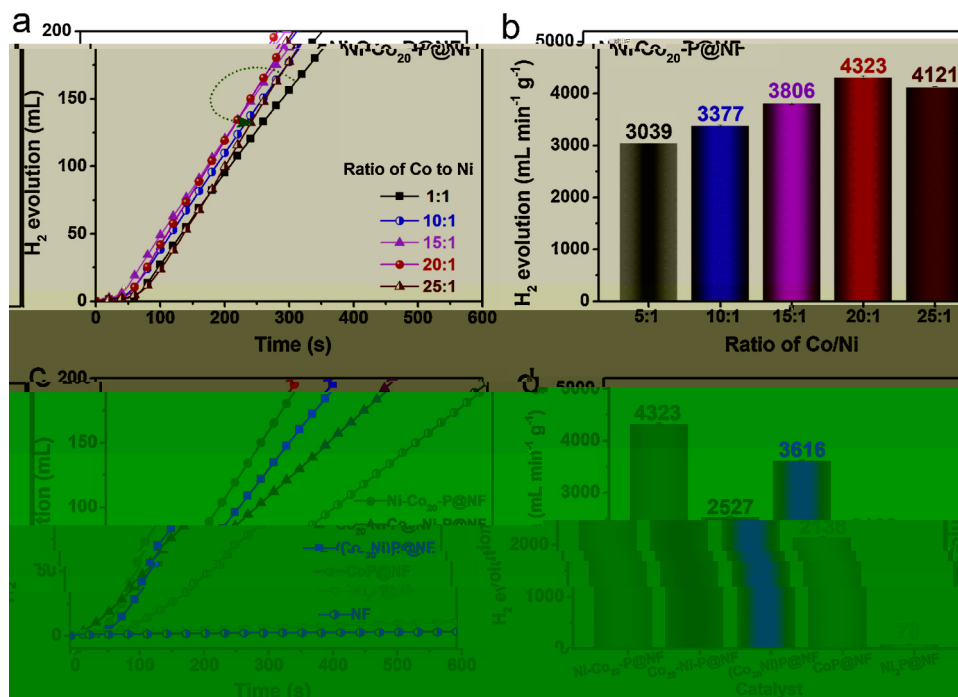
Fig. 4. (a) Stoichiometric H_2 evolution in 150 mM $NaBH_4$ + 0.4 wt % NaOH solution by Ni-Co_{20}-P@NF catalysts with different ratios of Co/Ni at 25 °C, and (b) the corresponding H_2 evolution rate values. (c) H_2 evolution by different catalysts at 25 °C, and (d) the summarized H_2 evolution rate values.

Ni-Co_{20}-P@NF catalyst still showed the best catalytic performance compared with the control catalysts prepared by different methods (Fig. 4c). We can see that the H_2 generation rate of Ni-Co_{20}-P@NF catalyst is approximate 1.71-, 1.20-, 2.02- and 55.42-fold higher than those of Co_{20}-Ni-P@NF, (Co_{20}Ni)P@NF, CoP@NF and Ni_2P@NF, respectively (Fig. 4d). Meanwhile, the high catalytic H_2 generation rate is also superior to most of the previously reported catalysts (**Table S4**). Such excellent catalytic activity is mainly caused by the synergistic effect between CoP and Ni_2P species combined with more catalytically active sites.

The temperature effect to the catalytic performance of Ni-Co_{20}-P@ NF and CoP@NF in the alkalized $NaBH_4$ solution are further investigated (Fig. 5a and **Fig. S6**). The results revealed that the catalytic performance increases with the increasing reaction temperatures. Moreover, the activation energies of Ni-Co_{20}-P@NF and CoP@NF are estimated to be 30.1 kJ mol^{-1} and 56.1 kJ mol^{-1} [40] respectively, and the activation energy of Ni-Co_{20}-P@NF is almost half of the that of CoP@NF (Fig. 5b) once again implies the strong positive synergy between Co and Ni species in the Ni-Co_{20}-P@NF. The reusability of Ni-Co_{20}-P@NF catalyst was evaluated by the continuous recycling experiments in alkalized $NaBH_4$ solution. The results show that it takes 5−8 min to collect 200 mL of H_2 from the 1st to the 5th use (Fig. 5c) as
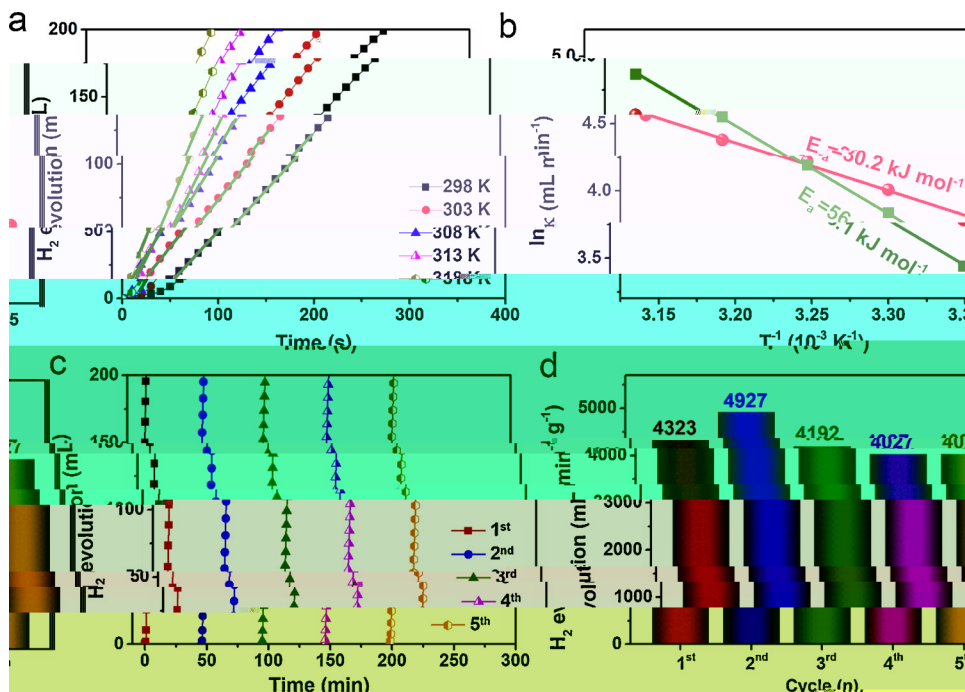

Fig. 5. (a) The relationship between the H_2 generation rate and applied temperatures of Ni-Co_{20}-P@NF. (b) The summarized Arrhenius plots for Ni-Co_{20}-P@NF and CoP@NF. (c) Recycling stability test of Ni-Co_{20}-P@NF catalyst in 150 mM $NaBH_4$ + 0.4 wt % NaOH at 25 °C. (d) The summarized specific H_2 generation rates in the different recycling test.

interests or personal relationships that could have appeared to influence the work reported in this paper.

Acknowledgements

Appendix A. Supplementary data

Supplementary material related to this article can be found, in the online version, at doi:https://doi.org/10.1016/j.apcatb.2019.118584.

References

[1] P. Brack, S.E. Dann, K.G.U. Wijayantha, P. Adcock, S. Foster, An old solution to a new problem? Hydrogen generation by the reaction of ferrosilicon with aqueous sodium hydroxide solutions, Energy Sci. Eng. 3 (2015) 535–540.

[2] L. Shao, H. Sun, L. Miao, X. Chen, M. Han, J. Sun, S. Liu, L. Li, F. Cheng, J. Chen, Facile preparation of NH_2-functionalized black phosphorene for the electrocatalytic hydrogen evolution reaction, J. Mater. Chem. A 6 (2018) 2494–2499.

[3] Y. Shi, B. Zhang, Recent advances in transition metal phosphide nanomaterials: synthesis and applications in hydrogen evolution reaction, Chem. Soc. Rev. 45 (2016) 1529–1541.

[4] Y. Zheng, Y. Jiao, A. Vasileff, S.Z. Qiao, The hydrogen evolution reaction in alkaline solution: from theory, single crystal models, to practical electrocatalysts, Angew. Chem. Int. Ed. 57 (2018) 7568–7579.

[5] H. Sun, Z. Yan, F. Liu, W. Xu, F. Cheng, J. Chen, Self-supported transition-metal-Based electrocatalysts for hydrogen and oxygen evolution, Adv. Mater. (2019) 1806326, https://doi.org/10.1002/adma.201806326.

[6] H. Du, R.-M. Kong, X. Guo, F. Qu, J. Li, Recent progress in transition metal phosphides with enhanced electrocatalysis for hydrogen evolution, Nanoscale 10 (2018) 21617–21624.

[7] E.J. Popczun, J.R. McKone, C.G. Read, A.J. Biacchi, A.M. Wiltrout, N.S. Lewis, R.E. Schaak, Nanostructured nickel phosphide as an electrocatalyst for the hydrogen evolution reaction, J. Am. Chem. Soc. 135 (2013) 9267–9270.

[8] F. Jing, Q. Lv, Q. Wang, K. Chi, Z. Xu, X. Wang, S. Wang, Self-supported 3D porous N-Doped nickel selenide electrode for hydrogen evolution reaction over a wide range of pH, Electrochim. Acta 304 (2019) 202–209.

[9] X. Lv, Z. Hu, J. Ren, Y. Liu, Z. Wang, Z.-Y. Yuan, Self-supported Al-doped cobalt phosphide nanosheets grown on three-dimensional Ni foam for highly efficient water reduction and oxidation, Inorg. Chem. Front. 6 (2019) 74–81.

[10] C. Sun, J. Zeng, H. Lei, W. Yang, Q. Zhang, Direct electrodeposition of phosphorus-doped nickel superstructures from choline chloride–Ethylene glycol deep eutectic solvent for enhanced hydrogen evolution catalysis, ACS Sustain. Chem. Eng. 7 (2018) 1529–1537.

[11] U.B. Demirci, About the technological readiness of the H_2 generation by hydrolysis of $B(-N)-H$ compounds, Energy Technol. 6 (2018) 470–486.

[12] A. Indra, T. Song, U. Paik, Metal organic framework derived materials: progress and prospects for the energy conversion and storage, Adv. Mater. 30 (2018) 1705146.

[13] D.-X. Xue, Q. Wang, J. Bai, Amide-functionalized metal–organic frameworks: syntheses, structures and improved gas storage and separation properties, Coord. Chem. Rev. 378 (2019) 2–16.

[14] N. Onishi, G. Laurenczy, M. Beller, Y. Himeda, Recent progress for reversible homogeneous catalytic hydrogen storage in formic acid and in methanol, Coord. Chem. Rev. 373 (2018) 317–332.

[15] K. Sordakis, C. Tang, L.K. Vogt, H. Junge, P.J. Dyson, M. Beller, G. Laurenczy, Homogeneous catalysis for sustainable hydrogen storage in formic acid and alcohols, Chem. Rev. 118 (2018) 372–433.

[16] M. Niermann, A. Beckendorff, M. Kaltschmitt, K. Bonhoff, Liquid Organic Hydrogen Carrier (LOHC)–Assessment based on chemical and economic properties, Int. J. Hydrogen Energy 44 (2019) 6631–6654.

[17] R. Zacharia, S. Rather, Review of solid state hydrogen storage methods adopting different kinds of novel materials, J. Nanomater. 2015 (2015) 1–18.

[18] L. Li, C. Xu, C. Chen, Y. Wang, L. Jiao, H. Yuan, Sodium alanate system for efficient hydrogen storage, Int. J. Hydrogen Energy 38 (2013) 8798–8812.

[19] E. Ianni, M.V. Sofianos, M.R. Rowles, D.A. Sheppard, T.D. Humphries, C.E. Buckley, Synthesis of $NaAlH_4$/Al composites and their applications in hydrogen storage, Int. J. Hydrogen Energy 43 (2018) 17309–17317.

[20] R. Palm, H. Kurig, J. Aruväli, E. Lust, $NaAlH_4$/microporous carbon composite materials for reversible hydrogen storage, Microporous Mesoporous Mater. 264 (2018) 8–12.

[21] J. Mao, D. Gregory, Recent advances in the use of sodium borohydride as a solid state hydrogen store, Energies 8 (2015) 430–453.

[22] U.B. Demirci, Impact of H.I. Schlesinger's discoveries upon the course of modern chemistry on $B-(N-)H$ hydrogen carriers, Int. J. Hydrogen Energy 42 (2017) 21048–21062.

[23] J. Guo, C. Wu, J. Zhang, P. Yan, J. Tian, X. Shen, T.T. Isimjan, X. Yang, Hierarchically structured rugae-like RuP_3–CoP arrays as robust catalysts synergistically promoting hydrogen generation, J. Mater. Chem. A 7 (2019) 8865–8872.

[24] L. Ouyang, W. Chen, J. Liu, M. Felderhoff, H. Wang, M. Zhu, Enhancing the regeneration process of consumed $NaBH_4$ for hydrogen storage, Adv. Energy Mater. 7 (2017) 1700299.

[25] L. Cui, Y. Xu, L. Niu, W. Yang, J. Liu, Monolithically integrated CoP nanowire array: an on/off switch for effective on-demand hydrogen generation via hydrolysis of $NaBH_4$ and NH_3BH_3, Nano Res. 10 (2016) 595–604.

[26] B. Li, L. Jiang, X. Li, Z. Cheng, P. Ran, P. Zuo, L. Qu, J. Zhang, Y. Lu, Controllable synthesis of nanosized amorphous MoS_x using temporally shaped femtosecond laser for highly efficient electrochemical hydrogen production, Adv. Funct. Mater. 29 (2019) 1806229.

[27] X. Cheng, D. Wang, J. Liu, X. Kang, H. Yan, A. Wu, Y. Gu, C. Tian, H. Fu, Ultra-small Mo_2N on SBA-15 as high-efficient promoter of low-loading Pd for catalytic hydrogenation, Nanoscale 10 (2018) 22348–22356.

[28] L.B. Huang, L. Zhao, Y. Zhang, Y.Y. Chen, Q.H. Zhang, H. Luo, X. Zhang, T. Tang, L. Gu, J.S. Hu, Self-Limited on-Site Conversion of MoO_3Nanodots into Vertically Aligned Ultrasmall Monolayer MoS_2 for Efficient Hydrogen Evolution, Adv. Energy Mater. 8 (2018) 1800734.

[29] W. Ahn, G. Park Moon, U. Lee Dong, H. Seo Min, G. Jiang, P. Cano Zachary, M. Hassan Fathy, Z. Chen, Hollow multivoid nanocuboids derived from ternary Ni-Co-Fe prussian blue analog for dual-electrocatalysis of oxygen and hydrogen evolution reactions, Adv. Funct. Mater. 28 (2018) 1802129.

[30] X. Wang, Z. Na, D. Yin, C. Wang, Y. Wu, G. Huang, L. Wang, Phytic acid-assisted formation of hierarchical porous CoP/C nanoboxes for enhanced Lithium storage and hydrogen generation, ACS Nano 12 (2018) 12238–12246.

[31] Y. Zhou, Y. Yang, R. Wang, X. Wang, X. Zhang, L. Qiang, W. Wang, Q. Wang, Z. Hu, Rhombic porous CoP_2 nanowire arrays synthesized by alkaline etching as highly active hydrogen-evolution-reaction electrocatalysts, J. Mater. Chem. A 6 (2018) 19038–19046.

[32] Z. Gao, F.Q. Liu, L. Wang, F. Luo, Hierarchical Ni_2P@$NiFeAlO_x$ nanosheet arrays as bifunctional catalysts for superior overall water splitting, Inorg. Chem. 58 (2019) 3247–3255.

[33] Z.-J. Chen, G.-X. Cao, L.-Y. Gan, H. Dai, N. Xu, M.-J. Zang, H.-B. Dai, H. Wu, P. Wang, Highly dispersed platinum on honeycomb-like NiO@Ni film as a synergistic electrocatalyst for the hydrogen evolution reaction, ACS Catal. 8 (2018) 8866–8872.

[34] R. Boppella, J. Tan, W. Yang, J. Moon, Homologous CoP/NiCoP heterostructure on N-Doped carbon for highly efficient and pH-Universal hydrogen evolution electrocatalysis, Adv. Funct. Mater. 29 (2018) 1807976.

[35] B. Wang, C. Tang, H.-F. Wang, X. Chen, R. Cao, Q. Zhang, A nanosized CoNi Hydroxide@Hydroxysulfide core-shell heterostructure for enhanced oxygen evolution, Adv. Mater. 31 (2019) 1805658.

[36] T. Zhang, K. Yang, C. Wang, S. Li, Q. Zhang, X. Chang, J. Li, S. Li, S. Jia, J. Wang, L. Fu, Nanometric Ni_5P_4 clusters nested on $NiCo_2O_4$ for efficient hydrogen production via alkaline water electrolysis, Adv. Energy Mater. 8 (2018) 1801690.

[37] I.K. Mishra, H. Zhou, J. Sun, K. Dahal, S. Chen, Z. Ren, Hierarchical CoP/Ni_5P_4/CoP microsheet arrays as a robust pH-universal electrocatalyst for efficient hydrogen generation, Energy Environ. Sci. 11 (2018) 2246–2252.

[38] C.-C. Hou, Q. Li, C. Wang, C.-Y. Peng, Q.-Q. Chen, H.-F. Ye, W. Fu, C.-M. Che, N. Lopez, Ternary Ni-Co-P nanoparticles and their hybrids with graphene as noble-metal-free catalysts to boost the hydrolytic dehydrogenation of ammonia-borane, Energy Environ. Sci. 10 (2017) 1770–1776.

[39] S.S. Williamson, P.A. Cassani, S. Lukic, B. Blunier, Chapter 6 - energy storage, in: M.H. Rashid (Ed.), Alternative Energy in Power Electronics, Butterworth-Heinemann, Boston, 2011, pp. 267–315.

[40] C. Wu, J. Zhang, J. Guo, L. Sun, J. Ming, H. Dong, Y. Zhao, J. Tian, X. Yang, Ceria-induced strategy to tailor Pt atomic clusters on cobalt-nickel oxide and the synergetic effect for superior hydrogen generation, ACS Sustain. Chem. Eng. 6 (2018) 7451–7457.

[41] Y. Shi, Y. Zhou, D.R. Yang, W.X. Xu, C. Wang, F.B. Wang, J.J. Xu, X.H. Xia, H.Y. Chen, Energy level engineering of MoS_2 by transition-metal doping for accelerating hydrogen evolution reaction, J. Am. Chem. Soc. 139 (2017) 15479–15485.

[42] L. Cui, Y. Xu, L. Niu, W. Yang, J. Liu, Monolithically integrated CoP nanowire array: an on/off switch for effective on-demand hydrogen generation via hydrolysis of $NaBH_4$ and NH_3BH_3, Nano Res. 10 (2017) 595–604.

[43] T. Liu, K. Wang, G. Du, A.M. Asiri, X. Sun, Self-supported CoP nanosheet arrays: a non-precious metal catalyst for efficient hydrogen generation from alkaline $NaBH4$ solution, J. Mater. Chem. A 4 (2016) 13053–13057.

[44] H.W. Liang, W. Wei, Z.S. Wu, X. Feng, K. Mullen, Mesoporous metal-nitrogen-doped carbon electrocatalysts for highly efficient oxygen reduction reaction, J. Am. Chem. Soc. 135 (2013) 16002–16005.

[45] H. Tan, J. Tang, J. Henzie, Y. Li, X. Xu, T. Chen, Z. Wang, J. Wang, Y. Ide, Y. Bando, Y. Yamauchi, Assembly of hollow carbon nanospheres on graphene nanosheets and creation of iron-nitrogen-Doped porous carbon for oxygen reduction, ACS Nano 12 (2018) 5674–5683.

[46] L. Zhou, J. Meng, P. Li, Z. Tao, L. Mai, J. Chen, Ultrasmall cobalt nanoparticles supported on nitrogen-doped porous carbon nanowires for hydrogen evolution from ammonia borane, Mater. Horiz. 4 (2017) 268–273.

[47] J. Jia, T. Xiong, L. Zhao, F. Wang, H. Liu, R. Hu, J. Zhou, W. Zhou, S. Chen, Ultrathin N-Doped Mo_2C nanosheets with exposed active sites as efficient electrocatalyst for hydrogen evolution reactions, ACS Nano 11 (2017) 12509–12518.

[48] D.J. Li, U.N. Maiti, J. Lim, D.S. Choi, W.J. Lee, Y. Oh, G.Y. Lee, S.O. Kim, Molybdenum sulfide/N-doped CNT forest hybrid catalysts for high-performance hydrogen evolution reaction, Nano Lett. 14 (2014) 1228–1233.

[49] X. Yang, A.-Y. Lu, Y. Zhu, M.N. Hedhili, S. Min, K.-W. Huang, Y. Han, L.-J. Li, CoP nanosheet assembly grown on carbon cloth: a highly efficient electrocatalyst for hydrogen generation, Nano Energy 15 (2015) 634–641.

[50] S.K. Singh, V.M. Dhavale, S. Kurungot, Low surface energy plane exposed Co_3O_4 nanocubes supported on nitrogen-doped graphene as an electrocatalyst for efficient water oxidation, ACS Appl. Mater. Interfaces 7 (2014) 442–451.